

# Electrochemical Evaluation of Corrosion on Borided and Non-borided Steels Immersed in 1 M HCl Solution

I. Mejía-Caballero, J. Martínez-Trinidad, M. Palomar-Pardavé, M. Romero-Romo, H. Herrera-Hernández, O. Herrera-Soria, and I. Campos Silva

(Submitted December 3, 2013; in revised form April 8, 2014; published online May 14, 2014)

In this study the corrosion resistances of AISI 1018 and AISI 304 borided and non-borided steels were estimated using polarization resistance and electrochemical impedance spectroscopy (EIS) techniques. Boriding of the steel samples was conducted using the powder-pack method at 1223 K with 6 h of exposure. Structural examinations of the surfaces of the borided steels showed the presence of a Fe<sub>2</sub>B layer with isolated FeB teeth on the AISI 1018 steel, whereas a compact layer of FeB/Fe<sub>2</sub>B was formed on the AISI 304 steel. Polarization resistance and EIS of the borided and non-borided steels surfaces were performed in a corrosive solution of 1 M HCl. The EIS data were analyzed during 43 days of exposure to the acid solution. Impedance curves obtained during this period for the borided and non-borided steels were modeled using equivalent electrical circuits. The results of both electrochemical techniques indicated that boride layers formed at the steel surfaces effectively protect the samples from the corrosive effects of HCl. The main corrosion processes observed on the boride layers were pitting and crevice corrosion.

**Keywords** borided steels, boriding, corrosion mechanism, EIS technique, polarization resistance

## 1. Introduction

Boriding is a thermochemical surface treatment in which boron diffuses into and combines with a substrate material to form a single- or double-phase metal-boride layer on the surface. Unlike many other surface treatments, hard boride layers can be developed on most alloys and metals via the diffusion of boron. The boriding of ferrous materials results in the formation of either a single (Fe<sub>2</sub>B) or double (FeB/Fe<sub>2</sub>B) layer with a well-defined composition. The thickness of each layer, also known as the case depth, affects the mechanical and chemical behavior of the borided steels and is dependent on the boriding temperature, treatment time, chemical composition of the steel, and the amount of boron that surrounds the sample surface (Ref 1, 2).

One of most important properties improved by boriding is corrosion resistance. Over the last 8 years, several studies have been performed in an attempt to estimate the corrosion resistance of borided steels using techniques other than continuous and cyclic immersion corrosion testing (Ref 3-10).

**I. Mejía-Caballero, J. Martínez-Trinidad, O. Herrera-Soria, and I. Campos Silva**, Instituto Politécnico Nacional, Grupo Ingeniería de Superficies, SEPI-ESIME, U.P. Adolfo López Mateos, Zacatenco, 07738 Mexico, DF, Mexico; **M. Palomar-Pardavé** and **M. Romero-Romo**, Universidad Autónoma Metropolitana, Av. San Pablo No. 180, Azcapotzalco, 02200 Mexico, DF, Mexico; and **H. Herrera-Hernández**, Universidad Autónoma del Estado de México, CU Valle de México, Ing. Industrial IIN, Blvd. Universitario s/n, 54500 Atizapán de Zaragoza, Edo. de México, Mexico. Contact e-mail: icampos@ipn.mx.

Presently, the electrochemical techniques are frequently employed to determine the corrosion resistance of surface-coated materials. Tavakoli and Mousavi Khoie (Ref 5) based their study to estimate the corrosion resistance of different grades of borided steels in a 3% NaCl solution. The electrochemical test (impedance spectroscopy technique) was carried out for 1, 4 h, and 2-4 days of exposure, in which the results showed that the presence of boride layers improved the corrosion rate within the range of boriding conditions. In addition, the study of Jiang et al. (Ref 6) proposed the polarization method and electrochemical impedance spectroscopy (EIS) technique to evaluate the corrosion behavior of low-carbon borided steels immersed in a 3.5 wt.% NaCl solution (the time of exposure of the borided steels to the acid solution was not specified in this study). The results of the electrochemical tests denoted that the presence of the Fe<sub>2</sub>B on the surface of the low-carbon borided steel enhanced the corrosion resistance compared with that not exposed to the thermochemical treatment. Similar results were obtained in the AISI 316 L SS boriding by the powder-pack method (Ref 10). The electrochemical experiments (Tafel extrapolation and linear polarization methods) were tested in 1 mol/dm<sup>3</sup> HCl, 1 mol/dm<sup>3</sup> NaOH, and 0.9% NaCl during 1 and 168 h at 310 K for each solution. The presence of FeB/Fe<sub>2</sub>B layers at the surface of borided stainless steel reduced the corrosion rate that was estimated for the HCl solution. However, in the NaOH and NaCl solutions, the corrosion resistance of the borided stainless steel denoted a decrease; it was found that the corrosion resistance of the borided samples tended to increase for longer periods of exposure in all solutions.

In the polarization resistance technique, a small potential perturbation,  $E$ , (typically of the order of  $\pm 10$  mV around the open circuit potential value, at a fixed potential scan rate) is applied to the working metal electrode and the resulting current response is recorded. The linear polarization resistance (LPR) is the ratio of the applied potential and the resulting current

response: such a resistance is inversely proportional to the corrosion current (Ref 11).

Electrical impedance spectroscopy (EIS) is a powerful electrochemical technique widely used in corrosion research. The analysis of the system's impedance measurements are generally carried out through the use of equivalent electrical circuits, that comprise passive elements namely: resistors, capacitors, inductors, and constant phase elements, to allow EIS data to be used to determine the electrochemical properties of the system, particularly those related to corrosion and its associated mechanisms.

EIS analysis can provide corrosion rate information and has the advantage of allowing measurements in solutions with low conductivity, such as those in which conventional DC techniques display large measurement errors (Ref 12-14).

In the present study, the corrosion resistances of AISI 1018 and AISI 304 borided and non-borided steels exposed to the 1 M HCl solution, a typical corrosive testing media, were evaluated using polarization resistance and EIS techniques. Boride layers were formed on the surfaces of the steels samples using the powder-pack boriding process at 1223 K during 6 h. From the polarization resistance technique, the corrosion current density ( $j_{\text{corr}}$ ) and the polarization resistance ( $R_p$ ) of all steels (borided and non-borided) were obtained using linear polarization methods. Moreover, the samples (borided and non-borided) were monitored by the EIS technique during 43 days immersed in the corrosive environment to evaluate the corrosion behavior and the surface corrosion mechanisms. Particularly, the corrosion behavior of the AISI 1018 and AISI 304 borided steels immersed in 1 M HCl for 43 days of exposure and with the aid of the EIS technique, has not yet been examined in the literature (Ref 3-10) as proposed in the present study.

Finally, equivalent electric circuits (EECs) were proposed for the analysis of the resulting impedance data.

## 2. Experimental Procedure

### 2.1 The Powder-Pack Boriding Process

The powder-pack boriding process was conducted on square commercial samples of AISI 1018 and AISI 304 steels. The chemical compositions of these steels are: 0.15-0.20 wt.% C, 0.6-0.9 wt.% Mn (AISI 1018 steel), and 0.08 wt.% C, 2 wt.% Mn, 1 wt.% Si, 18-20 wt.% Cr, 8-10 wt.% Ni, 0.045 wt.% P, 0.03 wt.% S (AISI 304 steel), respectively.

Prior to boriding, the specimens were polished, ultrasonically cleaned at room temperature in an alcohol solution and deionized water for 15 min, dried and stored in clean-room conditions.

Samples were embedded in a closed cylindrical case (AISI 304 steel) containing a  $B_4C$  Ekabor 2 fresh powder mixture. The powder-pack boriding process was performed at a temperature of 1223 K for 6 h. Once the treatment was complete, the container was removed from the furnace and slowly cooled to room temperature.

The borided samples were cross-sectioned and mounted in bakelite for metallographic preparation that consisted in: ground from 180 to 2000 grit SiC sand paper, and polished on 0.05  $\mu\text{m}$  colloidal silica suspension. In addition, polished samples were etched in a 4% Nital solution (AISI 1018 borided steel) and Vilella's reagent (AISI 304 borided steel), respectively. The depths of the boride layers were observed in a clear field by optical microscopy using a GX51 Olympus instrument.

The microstructure of the boride layers formed on the surface of the AISI 1018 and AISI 304 steels was verified by x-ray diffraction (XRD) applying regular  $2\theta - \omega$  scan procedure. An X'PERT PRO PANalytical instrument was used with  $\text{Cu K}_\alpha$  radiation at  $\lambda = 0.154 \text{ nm}$ .

### 2.2 Electrochemical Corrosion Evaluation

The electrochemical corrosion evaluation of borided and non-borided steels immersed in 1 M HCl was divided in two procedures: first, the behavior of the open circuit potential ( $E_{\text{OCP}}$ ) as a function of time, and polarization resistance experiments were performed on a commercial potentiostat-galvanostat (VersaSTAT4 equipment) with the aid of the VersaStudio Software for the experimental control and data acquisition. Second, the EIS technique was carried out using an IM6 electrochemical work station and a ZENNIUM potentiostat-galvanostat (ZAHNER instruments), respectively, coupled each to a respective PC running the Thales software.

All experiments were performed at room temperature and open circuit potential ( $E_{\text{OCP}}$ ) in a classical three-electrode cell with an AISI 316 L steel cylindrical rod as counter electrode and an Ag/AgCl mini-electrode as a reference electrode. The working electrode (the test specimen) was placed horizontally at the bottom of the cell and attached to an acrylic cylinder, leaving an exposed area of 1  $\text{cm}^2$ . Prior to electrochemical testing, the samples were immersed in an electrolyte solution for approximately 15 min to stabilize the open circuit potential ( $E_{\text{OCP}}$ ) at room temperature. The experimental setup for these tests is shown in Fig. 1.

Polarization resistance experiments were performed within the  $E_{\text{OCP}} \pm 10 \text{ mV}$  versus (Ag/AgCl) with a scan rate of 0.5 mV/s. Likewise, EIS measurements were recorded over 43 days of exposure to the acid solution, in which a sinusoidal input signal  $E_0 \sin(\omega t)$  was applied to the electrode system at a frequency of  $\omega$ . The frequency range was established from 8 MHz to 1 mHz (six frequency points per decade) by means of a sinusoidal AC potential perturbation with a 10 mV (rms) amplitude. Electrochemical parameters were estimated by fitting an appropriate EEC to the experimental data.

After the electrochemical tests, the samples were prepared metallographically (without mounting material) to analyze the surface corrosion mechanisms on the borided and non-borided steels using a scanning electron microscope (JEOL JXA-8200 equipment).

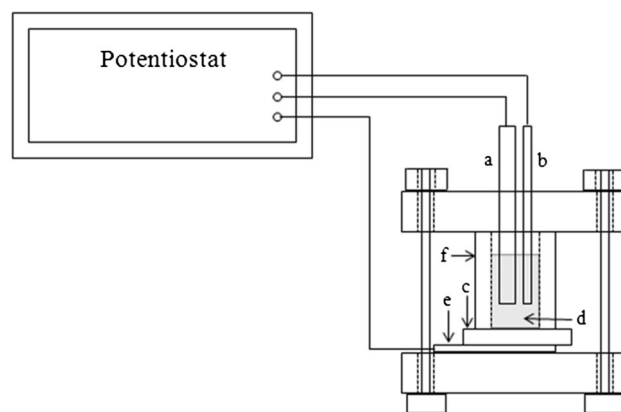


**Fig. 1** Experimental setup of the electrochemical tests. (a) Reference electrode, (b) counter electrode, (c) working electrode, (d) acid solution, (e) aluminum conductor, (f) standard cell

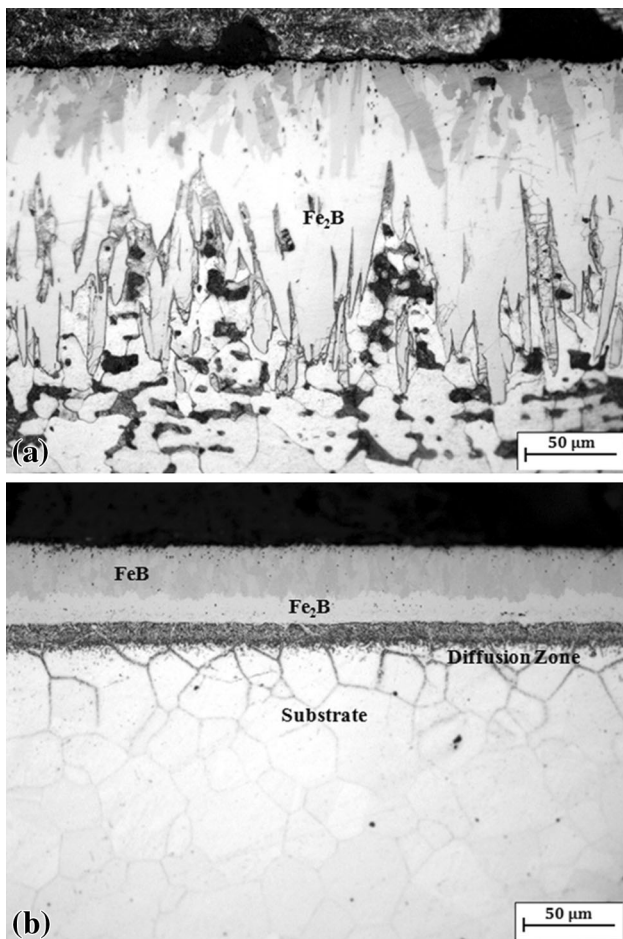


**Fig. 2** Cross-sectional views of borided steels: (a) AISI 1018 steel, (b) AISI 304 steel

### 3. Results and Discussions

#### 3.1 Microstructure of Borided Steels

Cross-sectional views of the AISI 1018 and AISI 304 borided steels are shown in Fig. 2. The boride layer that formed on the surface of the AISI 1018 steel displayed a saw-tooth morphology consisting of a  $\text{Fe}_2\text{B}$  layer with isolated FeB teeth that were verified by the XRD pattern presented in Fig. 3(a). The thickness of the  $\text{Fe}_2\text{B}$  layer was  $164 \pm 9 \mu\text{m}$ . The saw-toothed morphology of the boride layer can be explained by the existence of enhanced diffusion pathways in the  $\text{Fe}_2\text{B}$  crystal lattice (Ref 15).

For the AISI 304 borided steel, structural examination of the surface showed the presence of a FeB/ $\text{Fe}_2\text{B}$  layer with a total thickness of  $55 \pm 9 \mu\text{m}$ . As a result of a substitutional mechanism, chromium was found concentrated at the tips of the boride columns, indicating that the chromium inhibits the growth of the boride layers. Boron flux is decreased in zones of high chromium concentration; therefore, the columnar shape of the growth is reduced compared to the AISI 1018 borided steel (Ref 16-18). XRD performed on the surface of the AISI 304 borided steel (Fig. 3b) revealed the presence of the FeB- $\text{Fe}_2\text{B}$  layer. In addition, chromium reacts with boron forming interstitial compounds such as CrB,  $\text{Cr}_2\text{B}$ ; nickel diffuses a lesser extent into the boride layer and precipitates as a  $\text{Ni}_3\text{B}$  beneath the surface layer (Ref 19).

#### 3.2 Polarization Resistance Tests

Before the polarization resistance tests, the  $E_{\text{OCP}}$  as a function of time was measured for the borided and non-borided steels as shown in Fig. 4(a). For the entire set of experimental conditions, the  $E_{\text{OCP}}$  remained stable, and the more positive values corresponded to the borided samples. Notwithstanding, it is important to underline that in the case of the AISI 304 borided steel (Fig. 4a), the  $E_{\text{OCP}}$  tends toward more positive values (approximately  $-192 \text{ mV}$ ).

Figure 4(b) presents the variation of the current density,  $j$ , as a function of the corrosion overpotential ( $\eta_{\text{corr}} = E - E_{\text{OCP}}$ ) recorded from the polarization resistance tests for both borided and non-borided steels. For all the samples, the electrochemical reactions involved during the cathodic branch are related to the reduction of proton from the electrolyte and a small amount of dissolved oxygen from the environment. However, it is expected that the main contribution to the overall cathodic current comes from the former reaction due to the highly acidic medium.

The polarization resistances ( $R_p$ ) of all the samples were obtained directly from the plots depicted in Fig. 4(b) (Ref 20). In addition, the corrosion potentials ( $E_{\text{corr}}$ ) and corrosion current densities ( $j_{\text{corr}}$ ) for the respective materials were obtained from the intersection of anodic and cathodic Tafel regions using the extrapolation method (the values were graphically estimated from the respective  $E$  versus  $\log j$  plots).

From the results depicted in Table 1, the AISI 1018 steel showed an  $E_{\text{corr}}$  of  $-519 \pm 1 \text{ mV}$  with an  $j_{\text{corr}}$  of  $78.3 \pm 0.5 \mu\text{A}/\text{cm}^2$ . The microstructural change due to the presence of the  $\text{Fe}_2\text{B}$  layer on the surface of the AISI 1018 borided steel shifted the corrosion potential to a more positive value ( $E_{\text{corr}} = -413 \pm 2.3 \text{ mV}$ ) and a lower corrosion rate ( $j_{\text{corr}} = 21.1 \pm 0.8 \mu\text{A}/\text{cm}^2$ ). These results indicated that the strong protection was provided by the surface boride layer.

Similar results were obtained from the analysis of the AISI 304 borided and non-borided steels as shown in Table 1. The AISI 304 borided steel exhibits a  $j_{\text{corr}} = 2.05 \pm 0.02 \mu\text{A}/\text{cm}^2$ , which is lower than that in the AISI 304 steel ( $j_{\text{corr}} = 28.37 \pm 1.6 \mu\text{A}/\text{cm}^2$ ). The existence of the FeB/ $\text{Fe}_2\text{B}$  layer on the surface of the stainless steel establishes a more positive value of  $E_{\text{corr}}$  ( $-191 \pm 3 \text{ mV}$ ) compared to the AISI 304 non-borided steel ( $E_{\text{corr}} = -433 \pm 1.5 \text{ mV}$ ). These observations corroborate the beneficial effect of the borided layer formed on the AISI 304 steel toward corrosion protection.

The chemical composition of the substrate is also reflected in the  $j_{\text{corr}}$  and the  $E_{\text{corr}}$  values obtained from the AISI 1018 and AISI 304 borided steels. Alloying elements such as nickel and chromium in the AISI 304 borided steel are involved in surface anodic reactions that increase the corrosion potential in comparison to the AISI 1018 borided steel (Ref 8). This effect leads to an approximately 0.222 V difference in the  $E_{\text{corr}}$  values of the borided steels.

Using the  $j_{\text{corr}}$  values obtained in the polarization resistance tests for the borided and non-borided steels, the inhibiting efficiency (IE) of the boride layer can be estimated as (Ref 6):

$$\text{IE} = \frac{j_{\text{corr},0} - j_{\text{corr}}}{j_{\text{corr},0}} \times 100, \quad (\text{Eq 1})$$

where  $j_{\text{corr},0}$  is the current density of the substrate and  $j_{\text{corr}}$  is the current density of the borided steel. Based on Eq. 1, the inhibiting efficiency of the  $\text{Fe}_2\text{B}$  layer formed on the surface of the AISI 1018 steel is 73%, while the composite FeB/ $\text{Fe}_2\text{B}$  layer formed on the surface of the AISI 304 steel shows 93% efficiency.



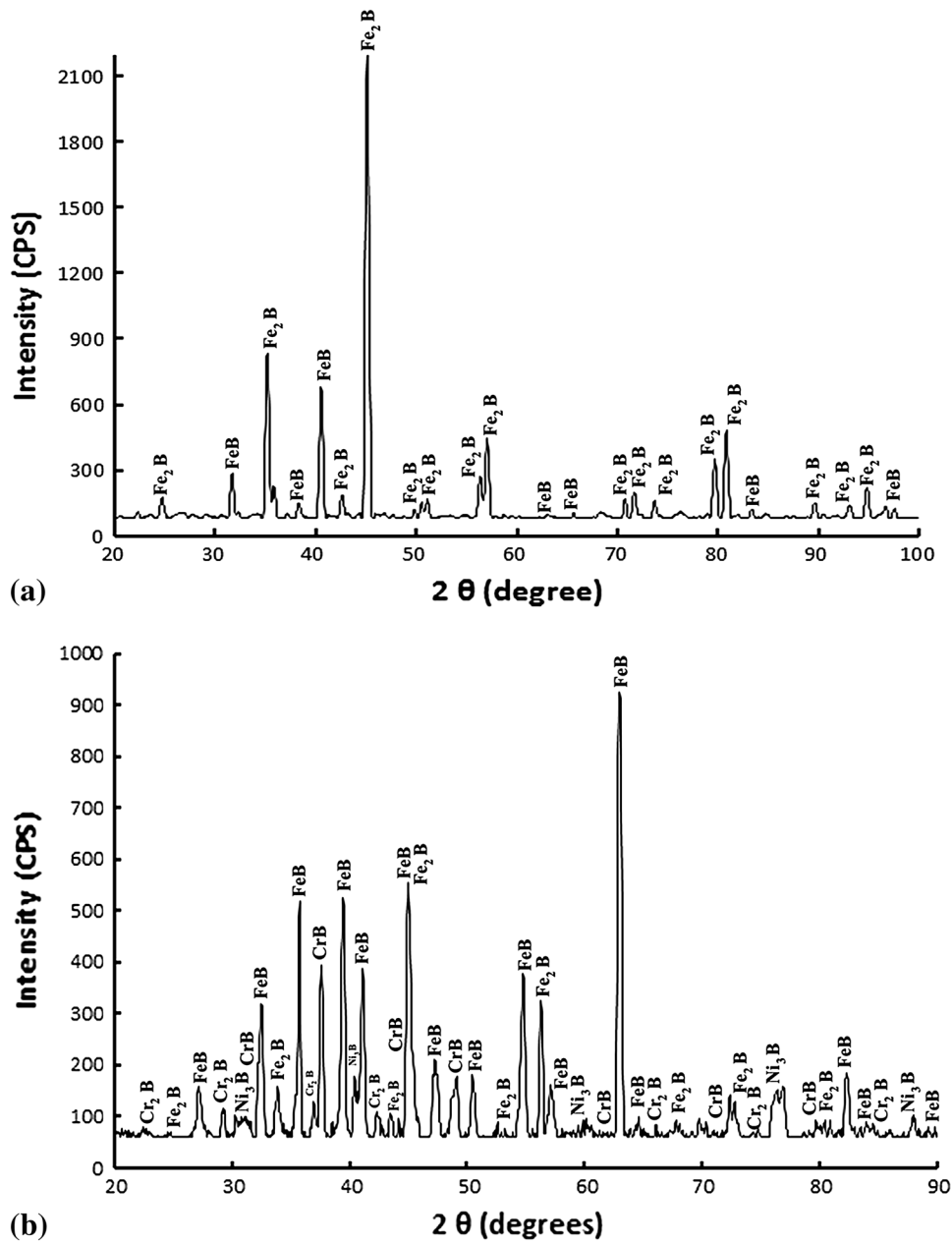


Fig. 3 X-ray diffraction patterns obtained on the surface of: (a) AISI 1018 borided steel, (b) AISI 304 borided steel

### 3.3 Electrochemical Impedance Spectroscopy Tests

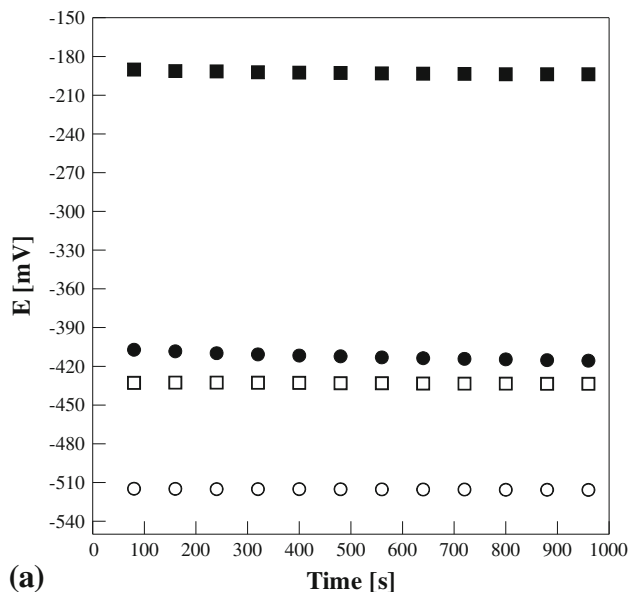
Figures 5 and 6 show the Nyquist plots obtained for borided and non-borided steels exposed to a 1 M HCl solution during 43 days. The electrolyte resistance ( $R_e$ ) is estimated from the impedance at high frequency  $|Z(j\omega)|_{\omega \rightarrow \infty}$ , where  $\omega$  is the radial frequency in an imaginary units  $j$ , while the sum of the charge transfer resistance ( $R_{ct}$ ) and the  $R_e$  is estimated from the impedance at low frequency  $|Z(j\omega)|_{\omega \rightarrow 0}$ . The difference between these two impedance values yielded the charge transfer resistance (Ref 4-6, 20).

The corrosion resistances of the borided and non-borided steels are directly proportional to the diameters of the arcs formed on the Nyquist plots (Ref 21).

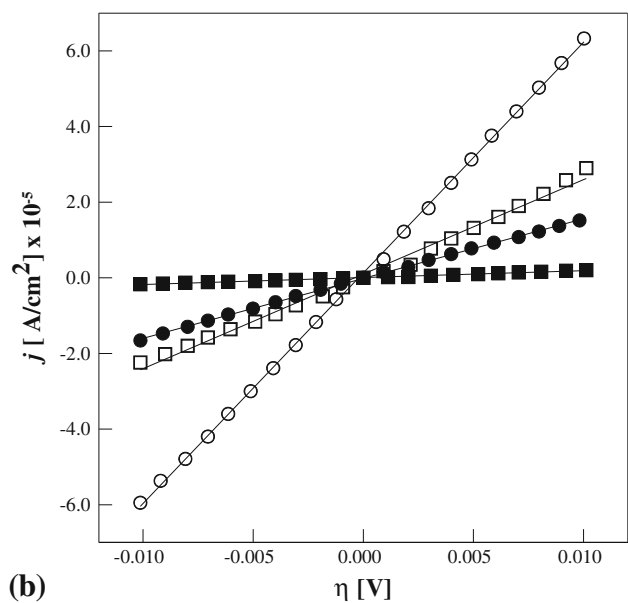
For the AISI 1018 borided steel, the corrosion resistance of the  $Fe_2B$  layer ( $R_c$ ) exhibited a maximum of  $16,784 \Omega \text{ cm}^2$  in

the second day of exposure and decreased to a reasonable corrosion resistance of  $1586 \Omega \text{ cm}^2$  by the 43rd day (Fig. 5a). In contrast, the non-borided AISI 1018 steel showed a resistance value ( $R_{cts}$ ) of  $164 \Omega \text{ cm}^2$  (Fig. 5b) during the second day of exposure, approximately 102 times smaller than that of the borided steel. The electrical parameters of the borided and non-borided AISI 1018 steels are summarized in Table 2. As shown from Table 2, the corrosion resistance of the AISI 1018 borided steel decreased for the 43rd day of exposure in the HCl solution, whereas the capacitance of the layer ( $C_c$ ) becomes more active.

The Nyquist plots obtained for the AISI 304 borided and non-borided steels are depicted in Fig. 6, and the results are summarized in Table 3. Figure 6(a) shows the high corrosion resistance reached by the AISI 304 borided steel due to the



(a)

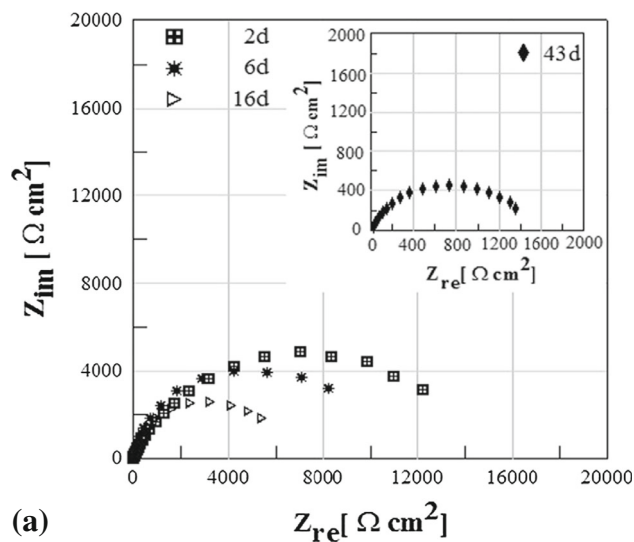


(b)

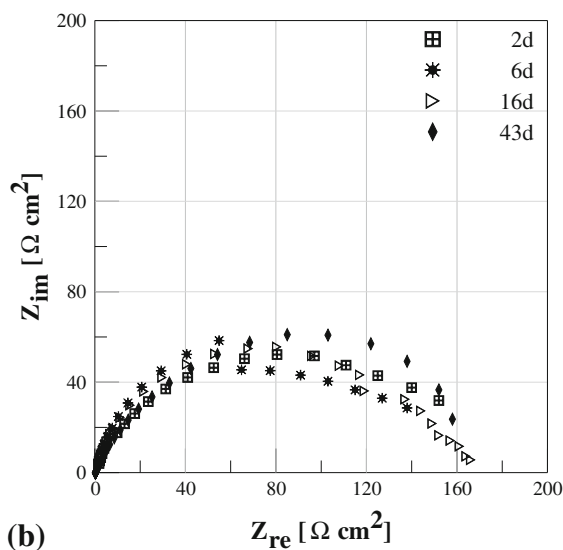
**Fig. 4** (a) Behavior of the open circuit potential,  $E_{OCB}$ , as a function of time for the different steel samples namely: (O) AISI 1018 steel,  $\square$  AISI 304 steel,  $\bullet$  AISI 1018 borided steel,  $\blacksquare$  AISI 304 borided steel. (b) Polarization resistance plots for the different steel samples stated in (a) immersed in 1 M HCl. The broken points were obtained by linear regression of the experimental points. (O) AISI 1018 steel,  $\square$  AISI 304 steel,  $\bullet$  AISI 1018 borided steel,  $\blacksquare$  AISI 304 borided steel

**Table 1 Results of the analysis of the polarization resistance plots**

Steel label	$R_p, \Omega \text{ cm}^2$	$j_{corr}, \mu\text{A}/\text{cm}^2$	$E_{corr}, \text{mV}$
AISI 1018 borided steel	$609 \pm 25$	$21 \pm 0.8$	$-413 \pm 2$
AISI 1018 steel	$164 \pm 1$	$78 \pm 0.5$	$-519 \pm 1$
AISI 304 borided steel	$6276 \pm 23$	$2.0 \pm 0.02$	$-191 \pm 3$
AISI 304 steel	$454 \pm 28$	$28 \pm 1.6$	$-433 \pm 1$



(a)



(b)

**Fig. 5** Experimental impedance plots (Nyquist format) for: (a) AISI 1018 borided steel and (b) AISI 1018 steel recorded during 43 days immersed in 1 M HCl

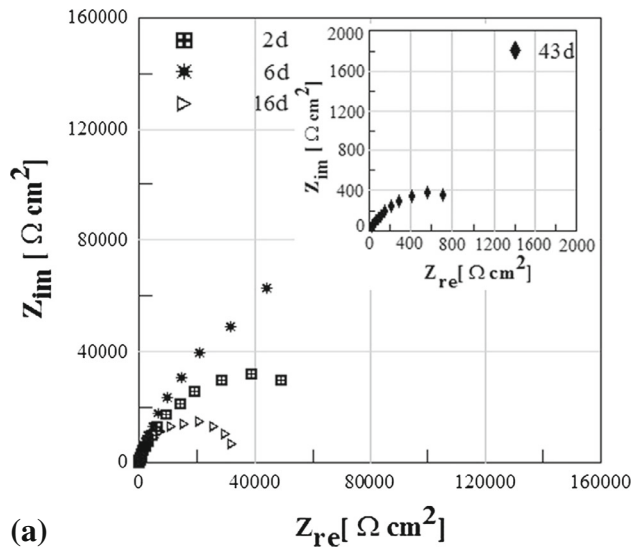
influence of the microstructure of the surface boride layer (FeB/Fe<sub>2</sub>B) and the high resistance of the pinholes ( $R_{pore}$ ). Defects such as pinholes over the layer are common in ceramic layers around the crevice and are likely to be a way where the acid media can infiltrate (Ref 22). The corrosion resistance of the AISI 304 borided steel reached a maximum value of  $290,210 \Omega \text{ cm}^2$  after 6 days of exposure to the corrosive environment, and it decreased to  $1793 \Omega \text{ cm}^2$  on the last day of exposure to the acid solution (Fig. 6a). On the 43rd day, the corrosion resistance of the AISI 304 non-borided steel ( $R_{cts}$ ) revealed a resistance value of  $821 \Omega \text{ cm}^2$  (Fig. 6b).

EIS data for both borided and non-borided steels are also displayed as Bode plots [ $\text{Log}[Z]$  versus  $\text{Log}(\text{Freq})$  and Phase angle versus  $\text{Log}(\text{Freq})$ ] in Fig. 7 and 8. Two-time constants can be represented for the borided steels: the first at high frequencies,  $\tau_c$ , that denotes the dielectric characteristics of the layer, and  $\tau_p$  developed at low frequencies and related to the porosity of the layer. The time constants are established as follows (Ref 23):

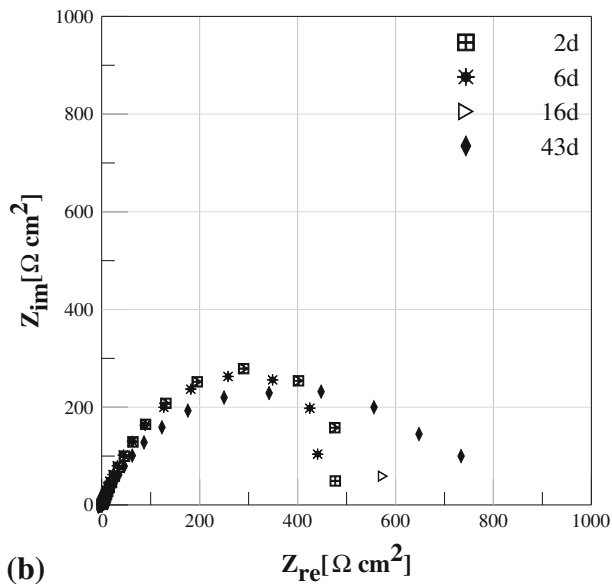
$$\tau_p = R_{\text{pore}}C_p; \quad \tau_c = R_cC_c, \quad (\text{Eq } 2)$$

where  $C_p$  is the capacitance of the pore.

As shown in Fig. 7(a), the behavior of the AISI 1018 borided steel at the beginning of the experiment (2nd day of



(a)



(b)

**Fig. 6** Experimental impedance plots (Nyquist format) for: (a) AISI 304 borided steel and (b) AISI 304 steel recorded during 43 days immersed in 1 M HCl

exposure) showed one phase constant attributed to the presence of the  $\text{Fe}_2\text{B}$  layer, in which the impedance reached a maximum value to the acid solution (Fig. 7b). From the 6th day of exposure, the presence of two-phase constants, one at high frequency ( $\text{Fe}_2\text{B}$  layer) and one at low frequency (porosity) was observed. In addition, the position of the peaks at high frequencies was decreased from the 16th day to the 43rd day of exposure to the 1 M HCl solution suggesting that the acid media through the pores has affected the dielectric characteristics of the boride layer.

Moreover, the behavior of the AISI 1018 steel revealed the presence of one phase constant at the beginning of the experiment (2nd day of exposure) as shown in Fig. 7c), which is assigned to corrosion-based electron charge transfer. The corrosion resistance on the 43rd day of exposure increased by approximately  $200 \Omega \text{ cm}^2$  (Fig. 7d) due to the accumulation of corrosion products on the steel surface

Figure 8(a) depicts the behavior of the AISI 304 borided steel exposed to the acid solution for the different exposure times. The low frequencies are associated with charge transfer processes in the electrochemical double layer, while the high frequencies are associated with the adsorption of the solution on the surface and consequent diffusional processes. The presence of two-phase constant at the beginning of the electrochemical test (2nd day of exposure) can be attributed to the presence of the boride layer and pores on the surface of the borided steel with high impedance values as shown in Fig. 8(b). The AISI 304 borided steel exhibited three-phase constants for the 43rd day of exposure related to the presence of the boride layer, the pores, and the steel substrate as shown in Fig. 8(a).

From the results of the AISI 304 steel presented in Fig. 8(c), one phase constant is developed during the 2nd to 16th days of exposure to the acid solution. During the first day of exposure, the corrosion of the AISI 304 steel was controlled by a charge transfer process, which is assigned to the corrosion-based electron charge transfer (Ref 24). From the 43rd day of exposure, two-phase constants were observed, which can be related to the presence of corrosion products on the steel surface. The impedance values obtained on the AISI 304 steel exposed to the acid solution for the different exposure times are depicted in Fig. 8(d).

The EEC models presented in Fig. 9(a) and (b) were applied to model the EIS data for the borided and non-borided steels, respectively. Different types of EEC models have been proposed in the literature for borided steels exposed to acid solutions (Ref 4-6, 25).

In this study, the EEC consists of the following elements for the borided steels: the electrolyte resistance  $R_e$ , the resistance of the boride layer ( $R_c$ ), the capacitance of the boride layer ( $C_c$ ), the resistance of the pore ( $R_{\text{pore}}$ ), and the capacitance of the pore ( $C_p$ ). In the case of the non-borided steels the EEC

**Table 2** Results of the analysis of Nyquist and Bode plots for the AISI 1018 borided and non-borided steels using EECs

Exposure time	AISI 1018 borided steel				AISI 1018 steel						
	$R_e, \Omega \text{ cm}^2$	$R_{\text{pore}}, \Omega \text{ cm}^2$	$C_p, \mu\text{F/cm}^2$	$n_p$	$R_c, \Omega \text{ cm}^2$	$C_c, \mu\text{F/cm}^2$	$n_c$	$R_e, \Omega \text{ cm}^2$	$R_{\text{cts}}, \Omega \text{ cm}^2$	$C_{\text{db}}, \mu\text{F/cm}^2$	$n_{\text{cts}}$
2d	6.3	50.4	182.2	0.90	16,784	13.6	0.76	5.0	164	349.3	0.84
6d	4.7	19.8	200.0	0.87	12,147	33.7	0.73	4.6	169	309.3	0.89
16d	3.8	12.2	357.1	0.84	8494	184.0	0.72	3.6	172	172.4	0.86
43d	2.7	8.5	483.8	0.82	1586	214.6	0.72	2.8	200	118.6	0.75

**Table 3** Results of the analysis of Nyquist and Bode plots for the AISI 304 borided and non-borided steels using EECs

Exposure Time	AISI 304 borided steel				AISI 304 steel							
	$R_e, \Omega \text{ cm}^2$	$R_{\text{pores}}, \Omega \text{ cm}^2$	$C_p, \mu\text{F/cm}^2$	$n_p$	$R_e, \Omega \text{ cm}^2$	$C_e, \mu\text{F/cm}^2$	$n_c$	$R_e, \Omega \text{ cm}^2$	$R_{\text{cts}}, \Omega \text{ cm}^2$	$C_{\text{dl}}, \mu\text{F/cm}^2$	$n_{\text{cts}}$	
2d	7.1	3089.8	36.1	0.83	109,140	22.0	0.79	3.57	529	69.79	0.86	
6d	4.9	1258.8	54.6	0.82	290,210	10.2	0.79	3.22	512	82.01	0.79	
16d	4.1	196.5	89.199	0.81	41,461	65.9	0.73	2.58	600	151.71	0.78	
43d	3.8	55.8	139.7	0.78	1793	72.6	0.72	1.96	821	167.49	0.76	

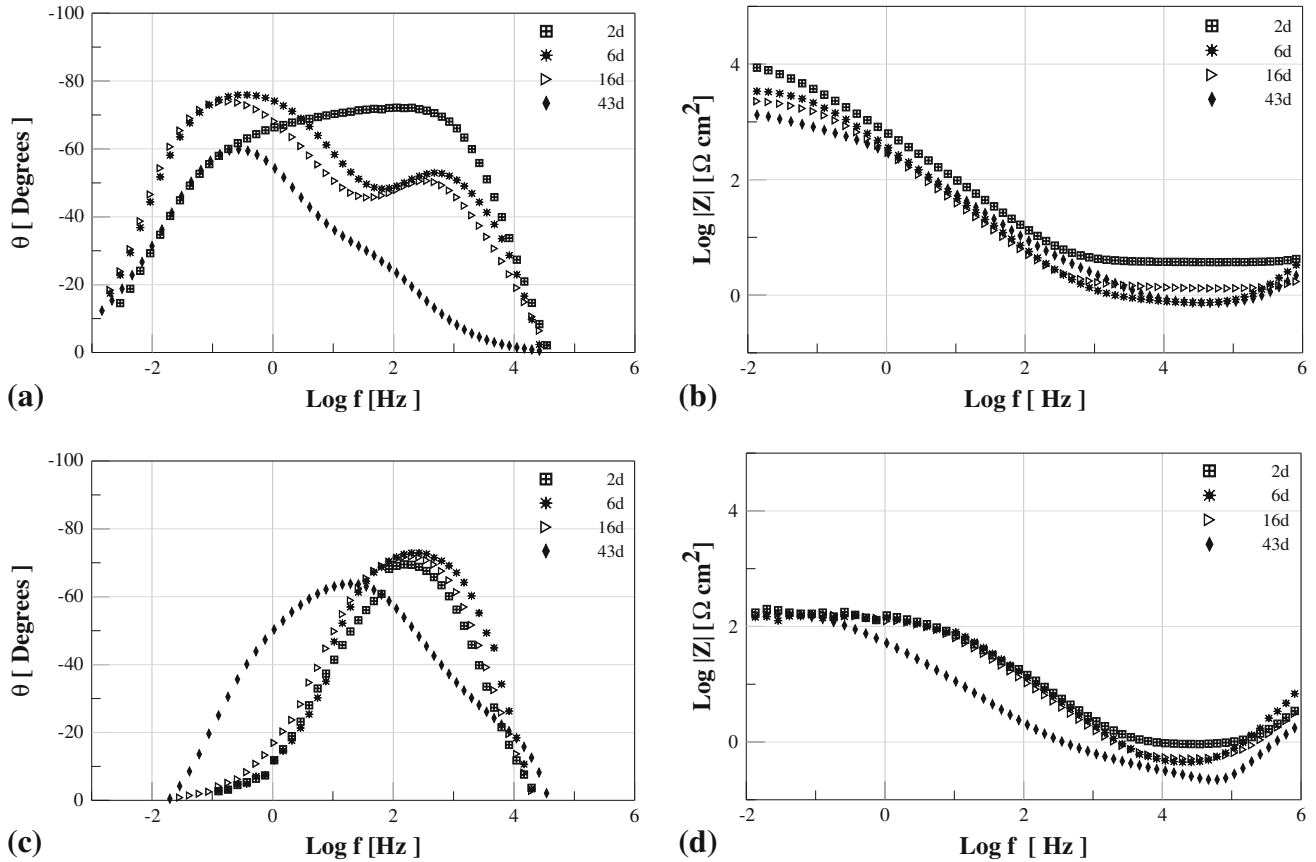


**Fig. 7** Experimental impedance plots (Bode format) for: (a, b) AISI 1018 borided steel and (c, d) AISI 1018 steel

consists of the electrolyte resistance, the resistance of the electron charge transfer of the substrate ( $R_{\text{cts}}$ ), and the electrochemical double layer of the substrate ( $C_{\text{dl}}$ ).

Constant phase elements (CPEs) are widely used in EIS data fitting to account for depressed semicircles. The capacitance ( $C$ ) is replaced with a CPE to model deviations from ideal dielectric behavior related to surface inhomogeneity. The CPE may be defined in impedance representation as follows:

$$Z_{\text{CPE}} = Z_0(j\omega)^n, \quad (\text{Eq 3})$$

where  $Z_0$  is an adjustable parameter (CPE constant), and  $n$  is the power that satisfies  $0 < n < 1$ , which is related to the surface texture of the electrode. Depending on  $n$ , CPE can represent a resistance ( $Z_{\text{CPE}} = R, n = 0$ ), capacitance ( $Z_{\text{CPE}} = C, n = 1$ ); Warburg impedance ( $Z_{\text{CPE}} = W, n = 0.5$ ), or inductance ( $Z_{\text{CPE}} = L, n = -1$ ) (Ref 26).

According to the results presented in Tables 2 and 3, the  $n$  values were closed to 1, thus, for the case of Fig. 9(a), the CPE is related to the capacitive characteristics of the porosity-layer system. From Fig. 9(b), the CPE is related to the charge transfer of the substrate.

The electromechanical parameters obtained from the EIS tests are useful in studying the porosity ( $P$ ) of the boride layers and can be established as follows (Ref 5):

$$P = \left( \frac{\tilde{R}_{\text{cts}}}{R_{\text{T}}} \right) \times 10^{|\Delta E_{\text{corr}}|}, \quad (\text{Eq 4})$$

where  $R_{\text{T}} = R_{\text{pore}} + R_{\text{c}}$  (Tables 2 and 3),  $\tilde{R}_{\text{cts}}$  is the mean resistance value of the non-borided steel during the 43 days of exposure to the acid media (for the AISI 108 steel was  $176 \Omega \text{ cm}^2$  and for the AISI 304 steel was  $616 \Omega \text{ cm}^2$ ), and  $|\Delta E_{\text{corr}}|$  is the difference in the corrosion potentials of the

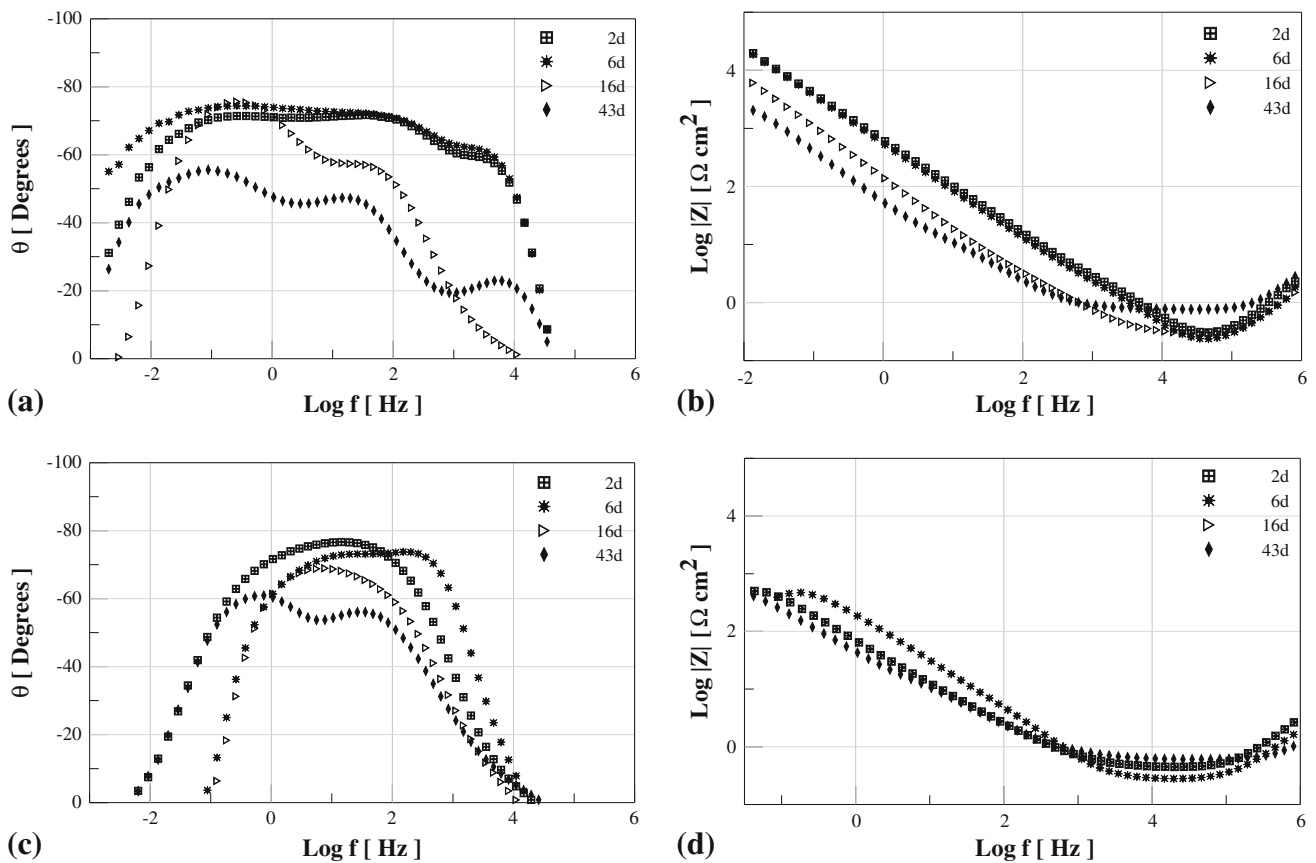


**Fig. 8** Experimental impedance plots (Bode format) for: (a, b) AISI 304 borided steel and (c, d) AISI 304 steel

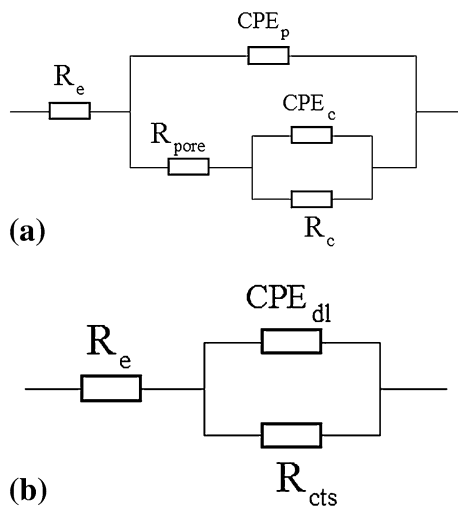


**Fig. 9** EECs used for the numerical fitting of the impedance data: (a) AISI 1018 and 304 borided steels, and (b) AISI 1018 and 304 non-borided steels

borided and non-borided steels evaluated per day in absolute values. The mean  $E_{\text{corr}}$  values for the AISI 1018 and AISI 304 steels during the 43 days of exposure were  $-0.508$  and  $-0.261$  V, respectively.

Porosity can weaken the interfacial material, providing an easy fracture path for adhesion failure. Local defects can form a direct path between a corrosive environment and the boride

layer, resulting in galvanic corrosion. Based on the results depicted in Table 4, corrosion resistance is enhanced by low porosity on the surface of the boride layers.

### 3.4 Corrosion Mechanisms

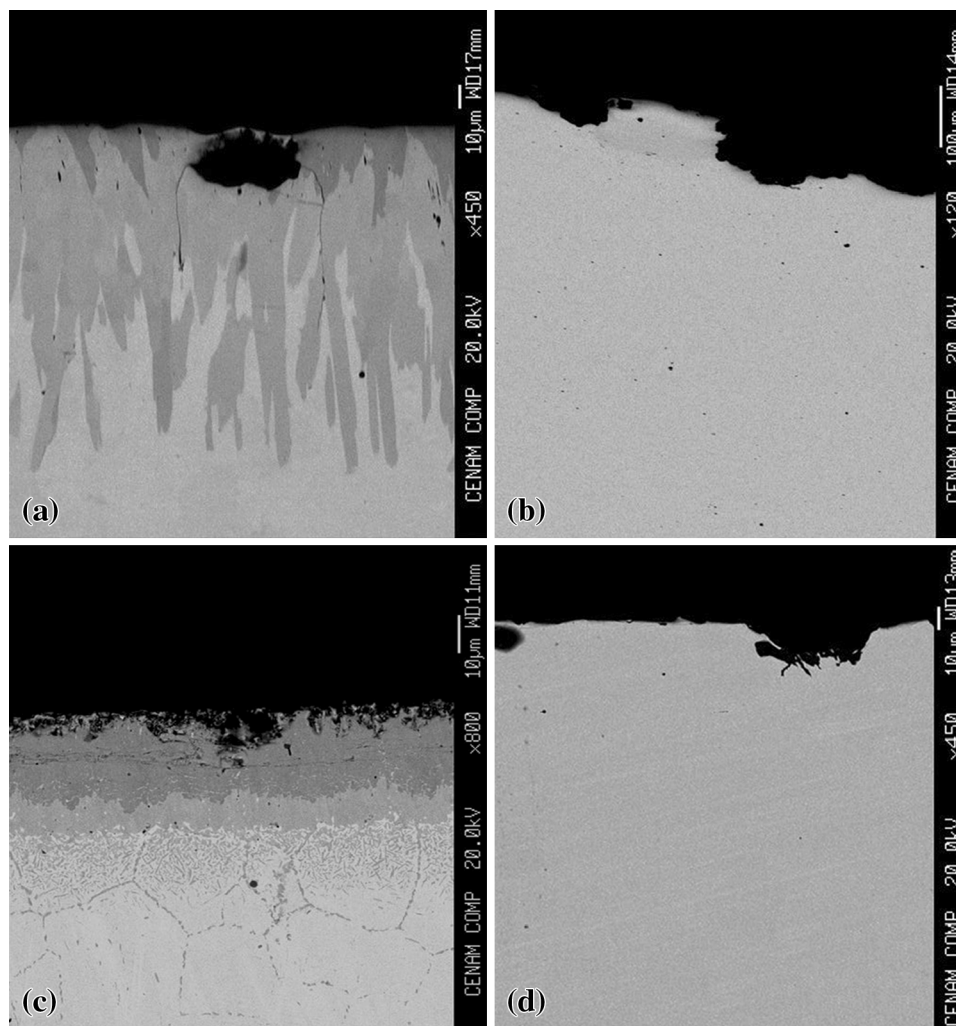
SEM analyses performed on the surfaces of the borided and non-borided steels (Fig. 10) after 43 days of exposure to the 1 M HCl solution showed the presence of both crevice (characteristic of metal-to-non-metal systems) and pitting corrosion mechanisms in the boride layers (Fig. 10a and c). The non-borided steels exhibit severe pitting (Fig. 10b and d), with considerably deeper pits than those observed in the borided steels.

The presence of defects, such as pores and flaws, on the surface of the borided steels results in the formation of galvanic cells at the defects because the boride layer is more electrochemically stable than the steel substrate. Once aggressive chloride ions penetrate the layer through these small channels, driven by capillary forces, the exposed area begins to experience anodic dissolution extending laterally along the interface between the boride layer and the steel substrate (Ref 9, 27). In this case, corrosion is vastly accelerated as the boride layer presents a large cathodic area in comparison to the very small exposed anodic substrate. Thus, the effective corrosion resistance of the boride layer/substrate system is related to the presence of defects in the boride layer, the adhesion between the layer and the steel substrate, and the passivation ability of the substrate (Ref 27, 28).



**Table 4** Porosity of the boride layers on AISI 1018 and AISI 304 borided steels determined from EIS data

Time	AISI 1018 borided steel		AISI 304 borided steel	
	$E_{corr}$ , V	Porosity, %	$E_{corr}$ , V	Porosity, %
2d	-0.265	0.01837	-0.147	0.00713
6d	-0.351	0.02085	-0.194	0.00246
16d	-0.375	0.02822	-0.118	0.02054
44d	-0.44	0.12964	-0.223	0.36350

**Fig. 10** Cross-sectional views obtained after 43 days immersion in 1 M HCl for: (a) AISI 1018 borided steel, (b) AISI 1018 steel, (c) AISI 304 borided steel, and (d) AISI 304 steel

#### 4. Conclusions

- From analyses of the plots obtained from polarization resistance and EIS electrochemical tests, the borided steels presented better corrosion resistance than non-borided steels.
- The AISI 304 borided steel showed higher corrosion resistance than the AISI 1018 borided steel due to differences in the chemical compositions of the substrates and the influence of the microstructure of the boride layer. Basically, alloying elements such as chromium and nickel are involved in the anodic reaction and increase the corrosion potential on the surface of the AISI 304 borided steel.
- Optimal corrosion resistance is a function of the low porosity exhibited by the boride layers. The surface porosity on the FeB/Fe<sub>2</sub>B layer is lower than that of the Fe<sub>2</sub>B layer formed on the AISI 1018 steel from the 2nd to the 16th day of exposure to the HCl solution.
- SEM images indicated crevice and pitting corrosion as the two major corrosion mechanisms in the borided steels, while pitting corrosion is the primary mechanism observed in the non-borided steels.

## Acknowledgments

This work was supported by Research Grant 150556 of the National Council of Science and Technology, and Research Grant 20130534 of the Instituto Politécnico Nacional in Mexico. The authors wish to thank the Centro Nacional de Metrología for their cooperation. M.P-P. and M.R-R. would like to thank SNI for the distinction of their membership and the stipend received.

## References

1. A.K. Sinha, "Boronizing", *Heat Treating 4*, 1st ed., ASM Handbook, Cleveland, OH, 1991
2. L.G. Yu, K.A. Khor, and G. Sundararajan, Boriding Mild Steel Using the Spark Plasma Sintering (SPS) Technique, *Surf. Coat. Technol.*, 2002, **157**, p 226–230
3. I. Campos, M. Palomar, A. Amador, R. Ganem, and J. Martínez, Evaluation of the Corrosion Resistance of Iron Boride Coatings Obtained by Paste Boriding Process, *Surf. Coat. Technol.*, 2006, **201**, p 2438–2442
4. I. Campos, M. Palomar, A. Amador, C. Villavelázquez, and J. Hadad, Corrosion Behavior of Boride Layers Evaluated by the EIS Technique, *Appl. Surf. Sci.*, 2007, **201**, p 9061–9066
5. H. Tavakoli and S.M. Mousavi Khoie, An Electrochemical Study of the Corrosion Resistance of Boride Coating Obtained by Thermo-reactive Diffusion, *Mater. Chem. Phys.*, 2010, **124**, p 1134–1138
6. J. Jiang, Y. Wang, Q. Zhong, Q. Zhou, and L. Zhang, Preparation of Fe<sub>2</sub>B Boride Coating on Low-Carbon Steel Surfaces and its Evaluation of Hardness and Corrosion Resistance, *Surf. Coat. Technol.*, 2011, **206**, p 473–478
7. G.K. Kariofillis, G.E. Kiourtsidis, and D.N. Tsipas, Corrosion Behavior of Borided AISI, H13 Hot Work Steel, *Surf. Coat. Technol.*, 2006, **201**, p 19–24
8. N. Suwattananont, R. Petrova, J.L. Zunino, D. Schmidt, Surface Treatment with Boron for Corrosion Protection, *Tri-Service Corrosion Conference*, Orlando, 2005, NACE 1
9. S.H. Alavi, C. Dehghanian, and P. Taheri, Investigation of Corrosion Behaviour of Carbon Steel Coated by Pulsed Plasma Electrolytic Boronising Technique in 3.5 wt% NaCl Aqueous Solution, *Surf. Eng.*, 2011, **27**, p 509–514
10. Y. Kayali, A. Buyuksagis, I. Gunes, and Y. Yalcin, Investigation of Corrosion Behaviors at Different Solutions of Boronized AISI, 316 L Stainless Steel, *Prot. Met. Phys. Chem. Surf.*, 2013, **49**, p 348–358
11. J. Fontana, *Corrosion Engineering*, 3rd ed., Mc Graw-Hill, New York, NY, 1986
12. S. Rossi, M. Fedel, F. Defloria, and M.C. del Vadillo, Localized Electrochemical Techniques: Theory and Practical Examples in Corrosion Studies, *C. R. Acad. Sci. II, C.*, 2008, **11**, p 984–994
13. Y. Huang, H. Shih, H. Huang, J. Daugherty, S. Wu, S. Ramanathan, C. Chang, and F. Mansfeld, Evaluation of the Corrosion Resistance of Anodized Aluminum 6061 Using Electrochemical Impedance Spectroscopy (EIS), *Corros. Sci.*, 2008, **50**, p 3569–3575
14. C. Liu, Q. Bi, A. Leyland, and A. Matthews, An Electrochemical Impedance Spectroscopy Study of the Corrosion Behavior of PVD Coated Steels in 0.5 NaCl Aqueous Solution: Part I. Establishment of Equivalent Circuits for EIS Data Modeling, *Corros. Sci.*, 2003, **45**, p 1243–1256
15. V.I. Dybkov, R. Siderko, L.V. Goncharuk, V.G. Khoruzha, and A.V. Samelyuk, Microstructure, Growth Kinetics, and Abrasive Wear Resistance of Boride Layers on Fe-30% Cr Alloy, *Powder Metall. Met. Ceram.*, 2013, **51**, p 518–530
16. E. García-Bustos, M.A. Figueroa-Guadarrama, G.A. Rodríguez-Castro, O.A. Gómez-Vargas, E.A. Gallardo-Hernández, and I. Campos-Silva, The Wear Resistance of Boride Layers Measured by the Four-Ball Test, *Surf. Coat. Technol.*, 2013, **215**, p 241–246
17. A.J. Ninham and I.M. Hutchings, On the Morphology of Thermochemically Produced Fe<sub>2</sub>B/Fe Interfaces, *J. Vac. Sci. Technol.*, 1986, **A4**, p 2827–2831
18. S. Taktak, Tribological Behaviour of Borided Bearing Steels at Elevated Temperatures, *Surf. Coat. Technol.*, 2006, **201**, p 2230–2239
19. I. Campos-Silva, M. Ortiz-Dominguez, O. Bravo-Bárceñas, M.A. Doñu-Ruiz, D. Bravo-Bárceñas, C. Tapia-Quintero, and M.Y. Jiménez-Reyes, Formation and Kinetics of FeB/Fe<sub>2</sub>B Layers and Diffusion Zone at the Surface of AISI, 316 Borided Steels, *Surf. Coat. Technol.*, 2010, **205**, p 403–412
20. W.J. Lorenz and F. Mansfeld, Determination of Corrosion Rates by Electrochemical DC and AC Methods, *Corros. Sci.*, 1981, **21**, p 647–672
21. N. Lin, M. Li, J. Zou, X. Wang, and B. Tang, Study on Fabrication and Corrosion Resistance of Ni-Based Alloy Coating on P110 Steel by Electro Spark Deposition, *J. Mater. Eng. Perform.*, 2012, **22**, p 1365–1370
22. C. Liu, Q. Bi, A. Leyland, and A. Matthews, An Electrochemical Impedance Spectroscopy Study of the Corrosion Behavior of PVD Coated Steels in 0.5 NaCl Aqueous Solution: Part II. EIS Interpretation of Corrosion Behavior, *Corros. Sci.*, 2003, **45**, p 1257–1273
23. H. Tavakoli, S.M. Mousavi Khoie, S.P.H. Marashi, and O. Bolhasani, Effect of Electrolyte Composition on Characteristics of Plasma Electrolysis Nitrocarburizing, *J. Mater. Eng. Perform.*, 2013, **22**, p 2351–2358
24. S.H. Ahn, Y.S. Choi, J.G. Kim, and J.G. Han, A Study on Corrosion Resistance Characteristics of PVD Cr-N Coated Steels by Electrochemical Method, *Surf. Coat. Technol.*, 2002, **150**, p 319–326
25. S.H. Alavi, C. Dehghanian, and P. Taheri, Investigation of Corrosion Behaviour of Carbon Steel Coated by Pulsed Plasma Electrolytic Boronising Technique in 3.5 wt%NaCl Aqueous Solution, *Surf. Eng.*, 2011, **27**, p 509–514
26. M. Palomar, M. Romero, H. Herrera, M.A. Abreu, N.V. Likhonova, J. Uruchurtu, and J.M. Juárez, Influence of the Alkyl Chain Length of 2-Amino-5-alkyl-1,3,4-thiadiazole Compounds on the Corrosion Inhibition of Steel Immersed in Sulfuric Acid Solutions, *Corros. Sci.*, 2012, **54**, p 231–243
27. H. Dong, Y. Sun, and T. Bell, Enhanced Corrosion Resistance of Duplex Coatings, *Surf. Coat. Technol.*, 1997, **90**, p 91–101
28. Y. Masiani, A. Medjahed, P. Gravier, and J.P. Crousier, Effect of a Titanium Underlayer on the Corrosion Behaviour of Physically Vapour Deposited Titanium Nitride Films, *Thin Solid Films*, 1992, **217**, p 31–37